Granular Matter
DOI 10.1007/s10035-006-0033-z

The spreading of a granular mass: role of grain properties and initial conditions

L. Staron · E. J. Hinch

Received: 23 January 2006
© Springer-Verlag 2006

Abstract We present 2D numerical simulations of the collapse and spreading of granular columns for which the final geometry of the deposit and the runout distance are studied. Both the effects of the initial geometry and the effects of the details of the interactions between the grains are investigated. The scaling of the runout distance shows both a linear and a power-law dependence on the aspect ratio of the initial column, in agreement with previous findings (Balmforth and Kerswell in J. Fluid Mech. 538, 399–428, 2004; Lajeunesse et al. in Phys. Fluids 17, 103302, 2005; Lube et al. in Phys. Rev. E 72, 041301, 2005; Staron and Hinch in J. Fluid Mech. 545, 1–27, 2005), and independently of the value of the inter-grain friction. The latter controls the prefactor of the scaling, the effective frictional properties of the flow, and its internal structure. The non-trivial mass distribution induced by the initial geometry of the column strongly influences the dissipation process, and is believed to controlthe power-law dependence of the runout distance on the column aspect ratio.

Keywords Granular flows · Runout · Effective friction · Numerical simulations · Contact dynamics

L. Staron (✉)
Department of Applied Mathematics and Theoretical Physics, University of Cambridge, CB3 0WA Cambridge, UK

Present address:
L. Staron
Laboratoire de Modélisation en Mécanique, Université Pierre et Marie Curie, 4 Place Jussieu, 75252 Paris Cedex 05, France
e-mail: staron@lmm.jussieu.fr

E. J. Hinch
Department of Applied Mathematics and Theoretical Physics, Center for Mathematical Sciences, University of Cambridge, Wilberforce Road, CB3 0WA Cambridge, UK
e-mail: E.J.Hinch@damtp.cam.ac.uk

1 Introduction

Many natural flows involving rocks, gravels and various debris can be tackled as granular provided the fluid trapped in the interstice (air, water possibly mixed with fines) plays no or little role in the overall dynamics [8]. Consequently, granular flows have been the subject of numerous works, either theoretical, experimental or numerical, with the definition of a proper rheology as a main objective [19,3,6,16]. The use of model granular material such as glass beads or calibrated sand in experiments, or the choice of basic interaction laws in numerical simulations, have considerably simplified the problem. In this framework, significant advance has been achieved, and various models could be successfully applied [18,1,7]. However, a comprehensive understanding of the dynamics of a collection of grains is still lacking, resulting mainly in the absence of reliable prediction in a number of flow configurations, including in first instance natural ones.

In this context, the issue of the flow runout, namely the final distance covered by a flowing mass of grains, is of great interest as it directly raises the question of predicting the destructive potential of natural flows. The nature of the material involved, the topography as well as the flow triggering mechanism are expected to play important roles. However, even highly idealized runout

experiments have shown a rich phenomenology which still remain only partially understood [14,10,2,21,22]. The experiment consists of releasing an initially confined column of granular material onto a horizontal plane and letting it spread freely until the flow comes to rest. The runout distance, namely the final distance eventually traveled by the flow, was shown to depend primarily on the aspect ratio a of the initial column. Linear and power-law scalings depending on the value of a are obtained both in 3D and 2D configurations. A simple energy balance assuming the dissipation of the initial potential energy by the constant friction of the flowing mass does not account for the power-law dependence [21]. On the contrary, assuming a simple balance between the friction force and the hydrostatic pressure at the front of the flow, together with simple dimensional arguments, allows one to recover the proper scalings [10]. Meanwhile details of the spreading dynamics could be achieved by means of discrete numerical simulations [21,22]. In particular, the role of the early stage of the collapse and the subsequent vertical dynamics was shown to be major [21]. As a result, a modification of the shallow-water equations to include this vertical dynamics at the inlet of the flow and using a basic rheology was sufficient to recover partly the correct behaviour [12]. Closer investigations of the internal structure of the flow were also performed [11,15]. However, the relation between the initial geometry, the structure of the flow and the value of the runout remain unclear.

In this contribution, we are interested in characterizing the influence of the material properties on the flow dynamics, and investigate how the details of the interaction between the grains interfere with the early dynamics induced by the initial geometry. Therefore, a similar numerical setup is used as in [21]. The influence of the value of the inter-grain friction is investigated. Surprisingly it does not affect the power-law scaling previously obtained for the runout distance. While the early dynamics of the collapse, following a free-fall, is only slightly affected by the inter-grain friction, the effective dissipation properties of the flow undergoes significant changes. Showing how the mass distribution in the flow affects the dissipation process, we propose the early free-fall dynamics to be at the origin of the power-law dependence. When investigating the internal structure of the flow, we show important differences induced by the inter-grain friction, in particular the formation of a static deposit during the spreading. The fact that differences in the interactions between the grains and in the details of the structure of the flow do not change the nature of the scalings satisfied by the runout is further discussed in the conclusion.

2 The simulations

2.1 The contact dynamics algorithm

The simulations were performed using the contact dynamics algorithm applied in two dimensions [17,9]. This algorithm assumes perfectly rigid grains interacting at contact by mean of a simple Coulomb friction law involving the coefficient of inter-grain friction μ. Moreover a Newton coefficient of restitution e controls energy exchanges during binary collisions. Beyond the fact that contact dynamics treats them as strictly non-smooth, these contact laws are essentially similar to those more commonly used in discrete simulations [22,4]. An important difference lies in the fact that contact dynamics tackles perfectly rigid grains, so that no soft contacts involving linear deformation and viscous dissipation are introduced. The behaviour of each grain is dictated by the equations of the dynamics and the interactions with the neighboring grains. The two coefficients μ and e are the only parameters introduced in the simulations. In the absence of any effect induced by the size, the shape and angularity of the grains (which are not tackled in this contribution), the value of both μ and e set the ability of the granular material to dissipate its energy.

2.2 The simulations set-up

We consider circular disks of mean diameter D and showing a slight uniform size-dispersity such that $(D_{\max} - D_{\min})/D = 0.4$. Columns of grains are built up by mean of random deposition in the gravity field between two vertical walls; R_0 designates their initial radius and H_0 their initial height, and $a = H_0/R_0$ is the aspect ratio. We have simulated six series of columns with $R_0/D = 10$, 15, 20, 30, 40 and 45, and with H_0/D varying between 20 and 240. The number of grains used in each column varies between 1,000 and 8,000, and the initial aspect ratio a varies between 0.2 and 20. At time $t = 0$, the column is allowed to collapse onto a horizontal plane on which grains of diameter D are glued to introduce roughness. The grains glued have the same properties as the grains in the columns, and induce contacts with the same value of μ and e as anywhere else in the flow. As a result of the collapse the granular mass spreads sideways and eventually comes to a rest as a heap of various shapes and runouts. In the following, the runout, namely the final distance run by the flow, is denoted R_∞. An illustration of the collapse process is displayed in Fig. 1 where layers of grains are dyed to show the deformations during the process.

The simulation setup is thus essentially the same as in [21], with the important addition of grains glued to

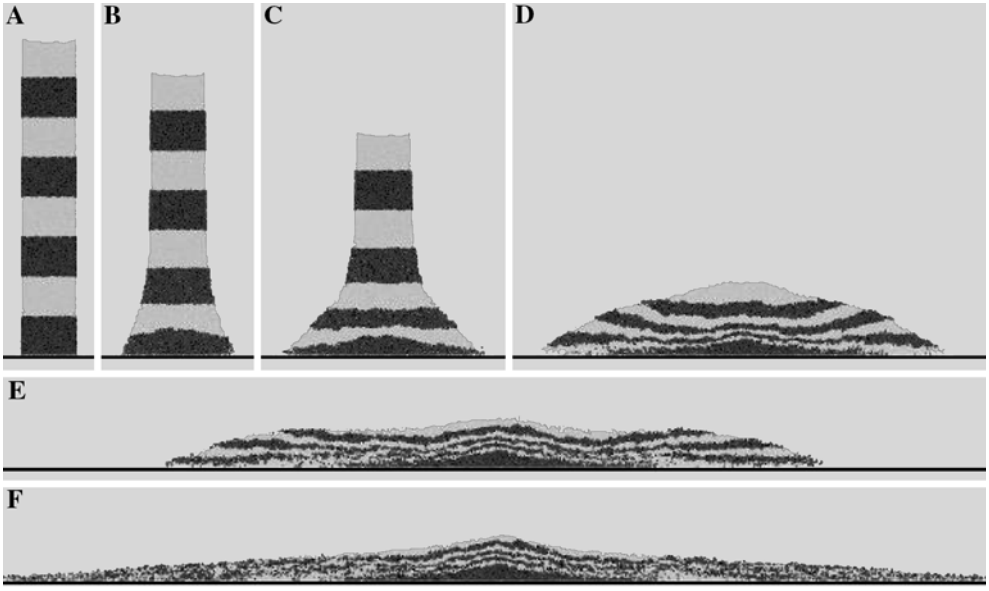

Fig. 1 Collapse of a column of initial aspect ratio $a = 11.7$ at successive instants of the spreading $t/T_\infty = 0, 0.15, 0.24, 0.41, 0.56$ and 1., where T_∞ is the total duration of the spreading, and for a restitution $e = 0.5$ and a inter-grain friction $\mu = 1$

the bottom, whose role is to change the dissipation at the base of the flow. Moreover, the systems presented hereafter explore a wider range of values for R_0/D and H_0/D (including those investigated in [21]).

In the following, the effect of the value of the inter-grain friction μ and of the coefficient of restitution e are investigated. However, the initial columns were all generated with the same value of both μ and e independently of the values taken by these two parameters during the flow. Hence, the initial columns used to study the influence of either e or μ are strictly similar, with a compacity around 0.82.

The results detailed hereafter were obtained from the analysis of 95 independent simulations.

3 Varying inter-grain friction and/or restitution?

Increasing the value of the inter-grain friction μ increases the amount of energy dissipated whenever two grains slip at contact. Moreover, it makes slipping motion more difficult to occur, and thus frustrates the motion of the whole collection of grains. Equivalently, low inter-grain friction leads to a lower rate of energy dissipation and thus to longer spreading. In the same way, a low restitution e will efficiently dissipate the energy during collisions, thus rapidly stopping the flow, while high restitution will allow grains to bounce further and further. The way the parameters μ and e affect the columns behaviour can be observed on Fig. 2a, b where an example of the sensitivity of the shape of the final deposit is displayed for different values of μ and e respectively.

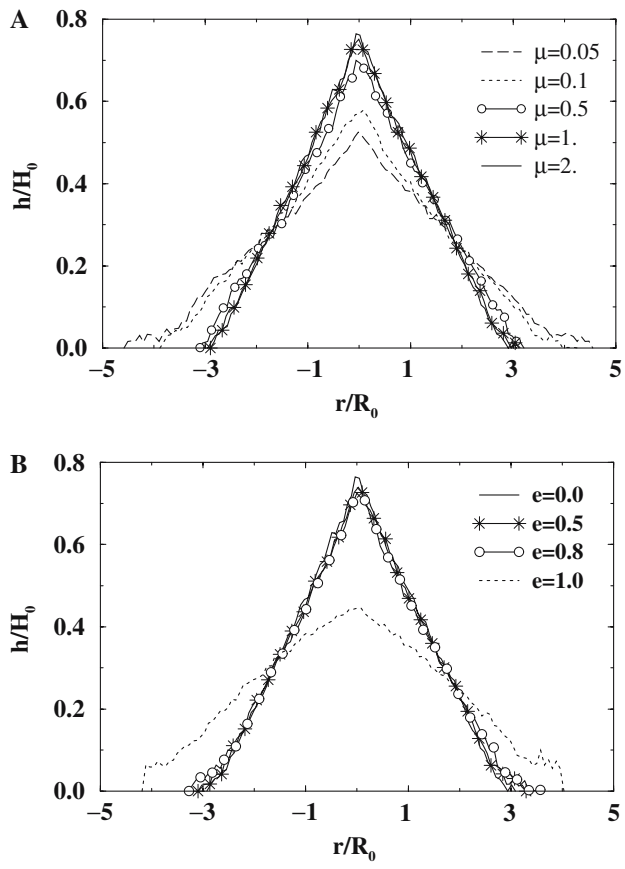

Fig. 2 Shape of the final deposit resulting from the collapse of a column of initial aspect ratio $a = 0.9$ **a** for a constant restitution between the grains $e = 0.5$ and for different values of the inter-grain friction $\mu = 0.05, 0.1, 0.5, 1$ and 2 and **b** for a constant inter-grain friction $\mu = 1$ and for different values of the restitution between the grains $e = 0, 0.5, 0.9$, and 1

For the sake of simplicity, we have considered a column with a relatively small initial aspect ratio $a = 0.9$ in order to avoid the non-trivial effects induced by the vertical dynamics which occurs for high aspect ratios.

From Fig. 2a, we observe that for large values of μ (i.e. between 0.5 and 2), the shape of the deposit remains nearly the same, namely the effective dissipation seems to saturate. On the contrary, for small to very small values of μ, the spreading of the mass considerably increases, resulting in larger runout and smaller final height. However the triangular shape of the pile is mainly conserved.

From Fig. 2b, we see that only very high values of the restitution, namely $e \to 1$, change the overall dynamics of the spreading and lead to a larger runout. In this case, the shape of the final deposit changes from a triangular heap to a more rounded one. This is due to the fact that high restitution changes the dynamics of the vertical collapse as much as the dynamics of the horizontal spreading, inducing a high agitation at the base of the column. In addition, bouncing grains persist at the front of the flow. Snapshots of these bouncing grains can be seen in Fig. 3 during the spreading for restitution $e = 0$, 0.8 and 1.

Note that generalizing these results to large aspect ratios is not straightforward due to the emergence and increasing role of the vertical dynamics. This is particularly true for the observations related to the coefficient of restitution e, which significantly changes the behaviour of the grains at the base of the columns. As for μ, its value seems to affect the vertical dynamics only in a marginal way, so that we are confident the observations presented for $a = 0.9$ should be valid for larger values of a. The influence of the value of a is precisely the subject of the forthcoming sections.

Since introducing high restitution e deeply affects the dynamics of the vertical collapse itself, investigating its influence on the horizontal spreading and the runout is difficult. Moreover, the cloud of bouncing grains induced by high e is a source of great uncertainty in the determination of the characteristics of the front of the flow (position, velocity...). Finally, the situation $e \to 1$ is rather unrealistic and does not apply to most granular flows, natural or experimental. Hence, in the following, we will not investigate the influence of e, and we set its value to $e = 0.5$ in all the simulations presented hereafter. On the other hand, we have seen that very small values of μ were necessary to affect significantly the spreading. In the coming sections, we will thus be interested in comparing the behaviour of two sets of simulations performed with a large value $\mu = 1$, and a very small value $\mu = 0.01$. Doing so, we expect to maximize the effects induced by inter-grain friction. However, intermediate values of μ will also be considered for evaluating the role of inter-grain friction on the effective dissipation properties.

4 The runout

4.1 The scaling

Investigating aspect ratios a ranging between 0.2 and 20, and considering the two following values of the

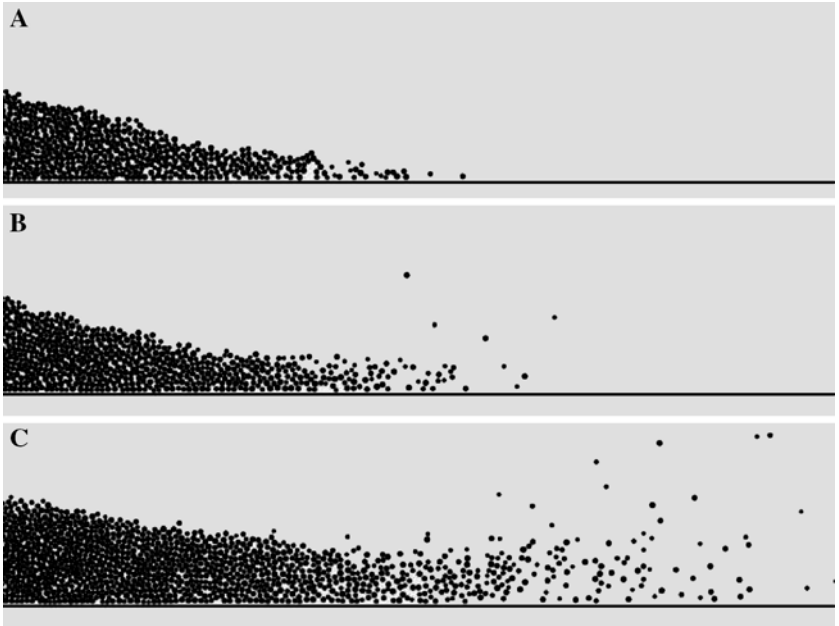

Fig. 3 Snapshots of the front of the flow resulting from the collapse of a column with $a = 0.9$ and $\mu = 1$, and $e = 0$ (*top* picture), 0.8 (*middle* picture) and 1. (*bottom* picture) taken at the same instant $t/T_0 \simeq 1$, where $T_0 = (2H_0/g)^{1/2}$. The grains glued to the bottom are not represented

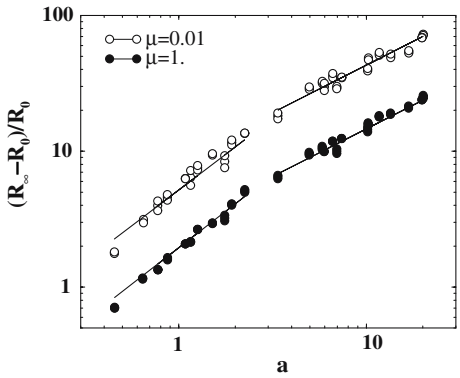

Fig. 4 Normalised runout distance $(R_\infty - R_0)/R_0$ as a function of the aspect ratio a for two values of the inter-grain friction $\mu = 0.01$ and $\mu = 1$

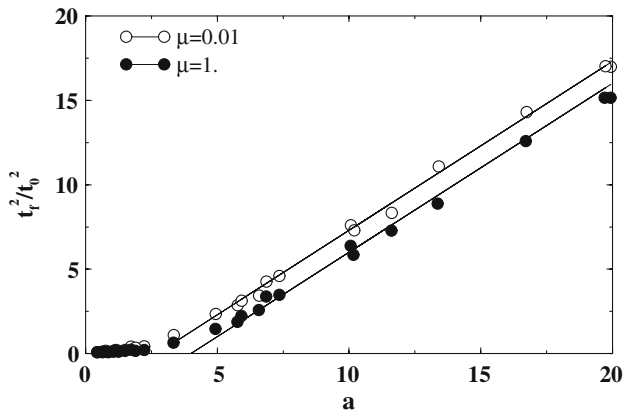

Fig. 5 Normalised free-fall time square $(t_f/t_0)^2$ as a function of the aspect ratio a for two values of the inter-grain friction $\mu = 0.01$ and $\mu = 1$

inter-grain friction $\mu = 0.01$ and $\mu = 1$, we are able to plot the normalised runout $(R_\infty - R_0)/R_0$ as a function of the aspect ratio a in Figure 4. We observe a very similar behaviour in the two cases, showing first a linear dependence followed by a power-law dependence, with an exponent α nearly constant. Figure 4 gives:

$$\frac{R_\infty - R_0}{R_0} \simeq \begin{cases} \lambda_1(\mu)\, a, & a \le a_0(\mu) \\ \lambda_2(\mu)\, a^{\alpha(\mu)}, & a \ge a_0(\mu), \end{cases} \tag{1}$$

with $\lambda_1(0.01) = 6.95$ and $\lambda_1(1) = 2.36$, and $\lambda_2(0.01) = 8.58$ and $\lambda_2(1) = 2.8$. The error bars (not represented) are not larger than the size of the symbols used. The exponent α is equal to 0.69 ± 0.015 and 0.70 ± 0.01 for $\mu = 0.01$ and $\mu = 1$. respectively, and can thus be considered independent of μ. The value of the aspect ratio a_0 characterizing the transition between linear and power-law dependence seems also to be independent of μ; from Fig. 4, $a_0 \simeq 2.5$. This behaviour is in agreement with previous experimental and numerical works [13,10,14,11,2,21].

The inter-grain friction changes the dissipation rate, as observed in [2]; the case $\mu = 0.01$ induces a runout nearly three times larger than the case $\mu = 1$. However this factor is small compared to the factor 100 between the two values of μ, which shows that dissipation during the collapse and the flow is still very efficient due to collisions between the grains.

The fact that inter-grain friction does not change the dependence of the runout on a even for very small values of μ suggests that the initial condition (the geometry of the initial column), dominates the spreading dynamics rather than the details of the interactions between the grains.

4.2 The free-fall dynamics

The role of the initial geometry on the spreading dynamics is apparent when analyzing the dynamics of the vertical collapse [21]. When tracking the position of the top of the column in the course of time, we show that it undergoes a free fall over a time interval t_f during which it remains undeformed. For each collapse we measure t_f with an accuracy of $\simeq D/(2gH_0)^{1/2}$, namely of the order of 10^{-3}s. Figure 5 displays the plot of $(t_f/t_0)^2$, where $t_0 = (2R_0/g)^{1/2}$, as a function of the aspect ratio a of the columns, and for the two values of the inter-grain friction $\mu = 0.01$ and $\mu = 1$. For small aspect ratios t_f is zero. For larger values of a, t_f becomes non-zero and we observe a linear dependence $t_f^2 \propto t_0^2 a$, which allows us to write:

$$t_f \simeq \begin{cases} \sqrt{\frac{2}{g}(H_0 - 2.7R_0)}, & \mu = 0.01 \\ \sqrt{\frac{2}{g}(H_0 - 4R_0)}, & \mu = 1. \end{cases} \tag{2}$$

These relations imply that the free-fall can occur only when the aspect ratio is over a certain value, here 2.7 or 4. Accordingly, we expect $a_0 = 2.7$ for $\mu = 0.01$ and $a_0 = 4$ for $\mu = 1$, where a_0 is the value of the aspect ratio characterizing the transition from linear to power-law dependence in the scalings (1), although these values are not obvious on Fig. 4 (certainly a much greater number of simulation would be necessary to characterize the transition without ambiguity). These predictions are slightly different from previous simulations performed on a smooth flat bottom [21], indicating an important effect of the roughness of the surface on the early stage of the collapse.

The relation (2) suggests that the transition between the power-law and the linear dependence given by the runout scalings (1) should result from a transition between a behaviour dominated by free-fall, and a behaviour where the spreading simply results from the failure of the edges of the column. In this last case, Coulombic friction would dominate the collapse dynamics: accordingly a_0 should depend on the inter-grain friction μ. For large aspect ratio however (namely $a >> a_0$), the collapse dynamics should be mainly independent of μ.

The total duration of the spreading T_∞ shows a linear dependence on $T_0 = (2H_0/g)^{1/2}$ independent of the value of the aspect ratio (Fig. 6):

$$T_\infty \simeq \begin{cases} 4.80T_0, & \mu = 0.01 \\ 2.30T_0, & \mu = 1. \end{cases} \tag{3}$$

In other words, the duration of the flow is related to the initial height of the column H_0 in the case of a collapse dominated by a Coulombic-like failure as well as in the case of a collapse dominated by a free-fall dynamics.

4.3 The effective friction: small aspect ratios

In the case of small aspect ratios, the columns undergo no free fall. The spreading mainly results from the failure of the edges, while the top of the column remains essentially undisturbed in the central areas [10,21]. Hence the amount of energy dissipated during the spreading δE can be easily recovered using the simple shape of the final deposit and volume conservation (see Fig. 7). The difference of potential energy between the initial and the final states gives

$$\delta E = \frac{1}{6} g\rho(R_\infty - R_0)H_0^2, \tag{4}$$

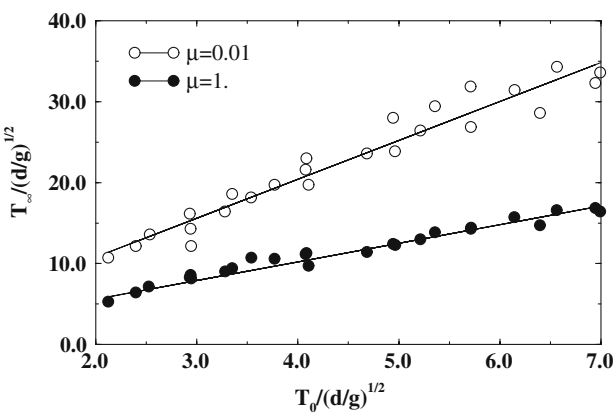

Fig. 6 Total duration of the spreading T_∞ as a function of the characteristic time T_0 for two values of the inter-grain friction $\mu = 0.01$ and $\mu = 1$, and for all values of a

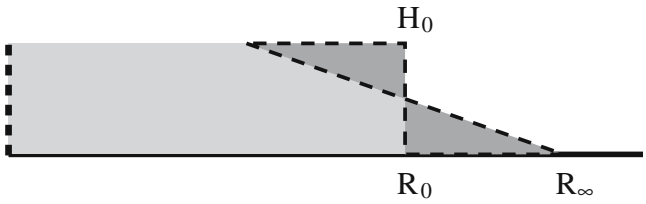

Fig. 7 Scheme of the collapse of a column with a small aspect ratio. The amount of energy δE lost in the process can be evaluated from the runout distance $R_\infty - R_0$

where ρ is the surfacic density of the packing. We suppose this energy to be dissipated by the work of friction forces W_μ over the total distance run by the center of mass G of the spreading material. Thus we consider the flow of the mass set in motion $\frac{1}{4}\rho(R_\infty - R_0)H_0$ over two thirds of the runout distance $2(R_\infty - R_0)/3$ (considering the triangular shape of the final deposit and the initial and final positions of the center of mass). Moreover we introduce the effective coefficient of friction μ_e characterizing the mean dissipation in the flow. The work of friction forces is thus

$$W_\mu = \frac{1}{6}\mu_e g\rho(R_\infty - R_0)^2 H_0. \tag{5}$$

Equating δE and W_μ gives $\mu_e(R_\infty - R_0) = H_0$. The scaling given in (1) leads directly to the relation $\mu_e = \lambda_1^{-1}$. This would give $\mu_e = 0.14$ for $\mu = 0.01$, and $\mu_e = 0.42$ for $\mu = 1$.

To check these predictions, we consider a set of simulations with aspect ratios $a = 0.21, 0.37, 0.55, 0.73$ and 0.9, and different values of the inter-grain friction $\mu = 0.01, 0.05, 0.1, 0.5, 1$ and 2. For each value of the aspect ratio, we compute the amount of energy δE actually dissipated during the spreading, and compare it with $W = \sum_{N_p} g m_p r_p$, where N_p is the total number of grains, m_p is their mass, and r_p is the total horizontal distance run by each of them. Considering the collapse of the column with the five values of the aspect ratio listed above, we check that δE and W are proportional for any value of μ; the coefficient of proportionality gives a measure of the effective coefficient of friction μ_e. This coefficient is essentially independent of the value of the aspect ratio a, so that the error bars on the evaluation of μ_e are very small. We are thus able to plot the value of μ_e as a function of the inter-grain friction μ (Fig. 8). The results are in agreement with the values predicted from the geometry of the final deposit. The behavior of μ_e can be nicely fitted by a power-law dependence on μ for small values of μ: $\mu_e = 0.425\mu^{0.20}$. This power-law dependence reflects an important "lubrication" of the granular mass in the sense that its mobility is extremely

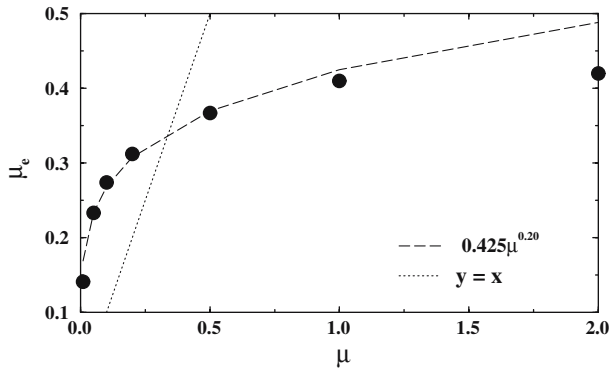

Fig. 8 Effective coefficient of friction μ_e (*full circles*) as a function of the inter-grain friction μ, evaluated from columns collapse with $a = 0.21$, 0.37, 0.55, 0.73 and 0.90. The *dashed line* shows a power-law fit, while the *dotted line* shows the unity line

enhanced by small reduction of the inter-grain friction. For large values of μ however, we observe a saturation, and the effective friction seems no longer to depend on the details of the inter-grain friction. Comparing the relation between μ_e and μ with the unity line, we observe that macroscopic friction is strongly reduced compared to the microscopic one for $\mu \geq 0.33$. Of course this behaviour is expected to be dependent on the shape of the grains, not investigated in the present work.

In the following, we will no longer consider small aspect ratios for which the scaling can be explained by a simple Coulomb-failure-like behavior. On the contrary, we will focus on large aspect ratio for which the effects of free fall are non-trivial.

5 Propagation of the flow: large aspect ratios

5.1 Velocity of the front

An example of the evolution of the normalised position of the front of the flow $(r - R_0)/(R_\infty - R_0)$ as a function of normalised time t/T_∞ is displayed in Fig. 9a during the collapse of a column with $a = 11.7$, and for the two values of the inter-grains friction $\mu = 0.01$ and $\mu = 1$. Figure 9b shows for the corresponding propagation the time evolution of the velocity of the front v, normalised by the characteristic velocity $(2gH_0)^{1/2}$. In both cases we first observe a period of acceleration followed by a period of deceleration, and no constant velocity propagation actually occurs. The flow never reaches a stationary regime where friction would balance the driving forces; and although a nearly stationary propagation could be reasonably approximated in the case $\mu = 1$, it remains short compared with the flow duration.

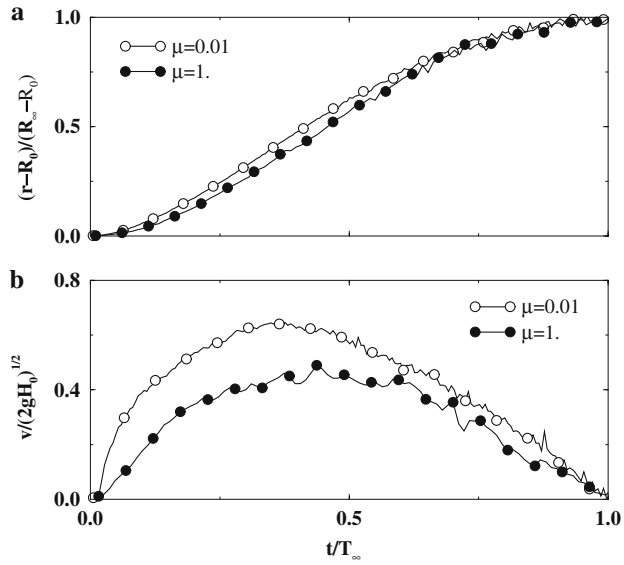

Fig. 9 **a** Position $r - R_0$ of the front of the flow normalised by the final runout $R_\infty - R_0$ and **b** velocity of the front v normalised by the typical velocity $(2gH_0)^{1/2}$ as a function of the time normalised by the spreading duration T_∞ for the two values of the inter-grain friction $\mu = 0.01$ and $\mu = 1$ and for $a = 11.7$

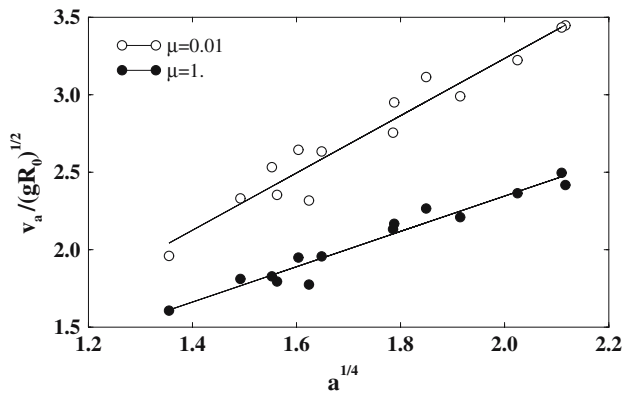

Fig. 10 Maximum velocity v_a reached by the front of the flow for aspect ratios $a > 2.5$, and for the two values of the inter-grain friction $\mu = 0.01$ and $\mu = 1$

We denote v_a the maximum value reached by the front velocity v; v_a shows the following dependence (Fig. 10):

$$v_a/(gR_0)^{1/2} \simeq \begin{cases} 1.84a^{1/4}, & \mu = 0.01 \\ 1.14a^{1/4}, & \mu = 1. \end{cases} \tag{6}$$

We propose no explanation of this dependence. Using the velocity v_a as an approximation of the velocity of the front during the total duration of the spreading T_∞, we can make a prediction of the runout: $(R_\infty - R_0) \propto v_a T_\infty \propto v_a T_0$, which gives directly $(R_\infty - R_0)/R_0 \propto$

$a^{3/4}$. The exponent $3/4 = 0.75$ is slightly larger than the exponent actually observed in the scalings $\alpha \simeq 0.70$ (Fig. 4). This difference might be due to the fact that assuming the front velocity to behave like v_a, i.e. assuming the acceleration phase to control the runout, does not accurately describe the front propagation. Note that this result does not match previous measurements showing $v \propto (gR_0)^{1/2}$ [10,21] obtained by the analysis of the shape of the front trajectory $r(t)$, likely less accurate.

The relative duration of the acceleration and deceleration periods show a systematic dependence on the inter-grain friction μ. As can be seen from Fig. 9b, the deceleration phase is longer for weak inter-grain friction.

5.2 The mass distribution

The sideways spreading of the grains is initiated by the vertical acceleration of the grains following a free-fall dynamics. Accordingly the flow is fed by an increasing flux of grains of increasing energy. The consequence of this initial condition is a non-trivial mass and energy distribution in the flow while it is propagating.

To compare the mass distribution in the flow in the course of time, we consider vertical sections of fixed width $dx = 5D$. The flow is thus divided between R_0 and $r(t)$ into $n_k = \mathrm{int}((r(t) - R_0)/dx)$ sections situated at $x_k = kdx$ of the base of the column. The mass of grains $m(x_k)$ in each of these sections is computed in the course of time. This gives the mass distribution in the flow at each instant t of the spreading. To compare the mass distribution in the course of time, $m(x_k)$ is normalised by the mass corresponding to a uniform distribution at instant t. We denote m_k this normalised mass at the position x_k:

$$m_k = \frac{m(x_k) \times n_k}{\sum_l m(x_l)}. \tag{7}$$

In Fig. 11, m_k is plotted as the function of the normalised position in the flow $x_k/(r(t) - R_0)$ every 1/80 s for a column with an aspect ratio $a = 11.7$ and an inter-grain friction $\mu = 0.01$. We observe the formation of a bump corresponding to the propagation of a mass wave in the flow, which eventually vanishes during the deceleration phase. For comparison, Fig. 12 display the normalised mass distribution in the flow resulting from the collapse of a column with $a = 0.73$ and for the same value of μ; no bump is observed and the flow keeps a triangular shape all through the spreading.

One effect of this bump is to propagate the momentum released by the column free-fall to the front of the flow. This phenomenon is illustrated in Fig. 13 where the profile of the momentum p normalised by $m_0(2gH_0)^{1/2}$ is plotted as a function of the normalised position in the flow $x_k/(r(t) - R_0)$ at different instant of the spreading, for a column of aspect ratio $a = 11.7$ and an inter-grain friction $\mu = 0.01$. We see the maximum of momentum propagating outwards from the base of the column to the front of the flow. We denote r_m its position. In Fig. 14, $(r_m - R_0)/R_0$ is compared with the normalised position

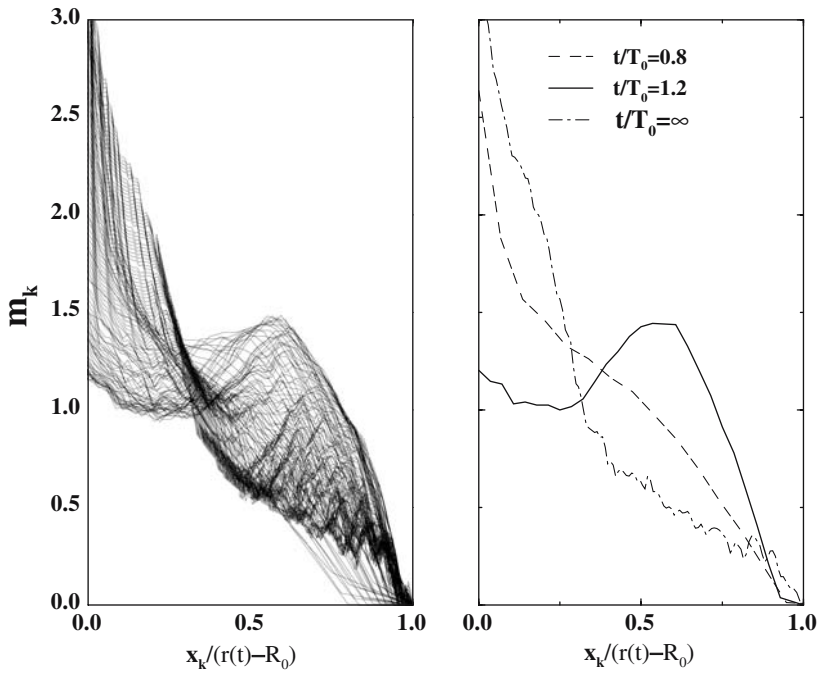

Fig. 11 Normalized mass distribution during the collapse and the spreading of a column with aspect ratio $a = 11.7$ plotted every 0.0125 s (left-hand side graph) and at three different moments of the spreading (right-hand side graph). The inter-grains friction is $\mu = 0.01$

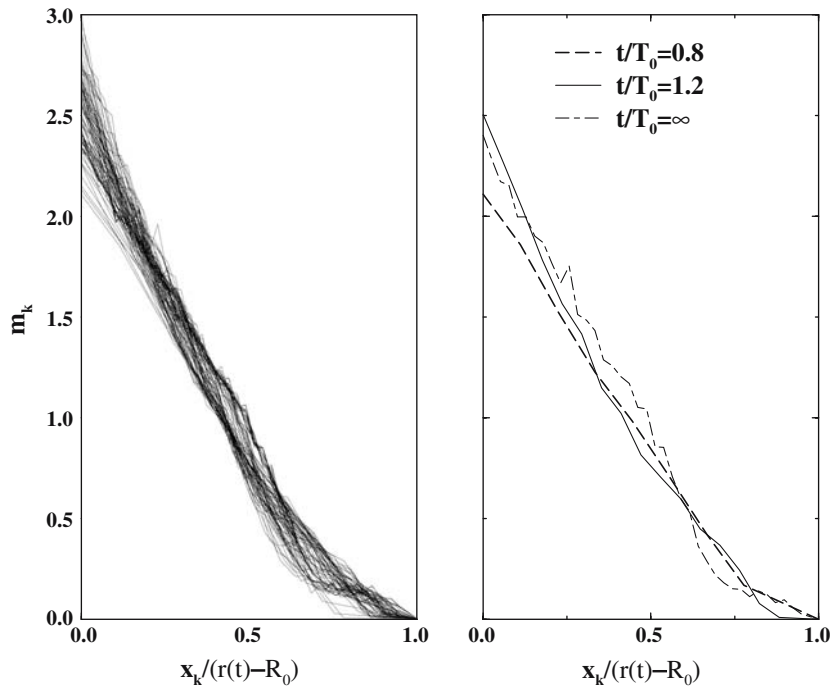

Fig. 12 Normalized mass distribution during the collapse and the spreading of a column with aspect ratio $a = 0.75$ plotted every 0.0125 s (left-hand side graph) and at three different moments of the spreading (right-hand side graph). The inter-grains friction is $\mu = 0.01$

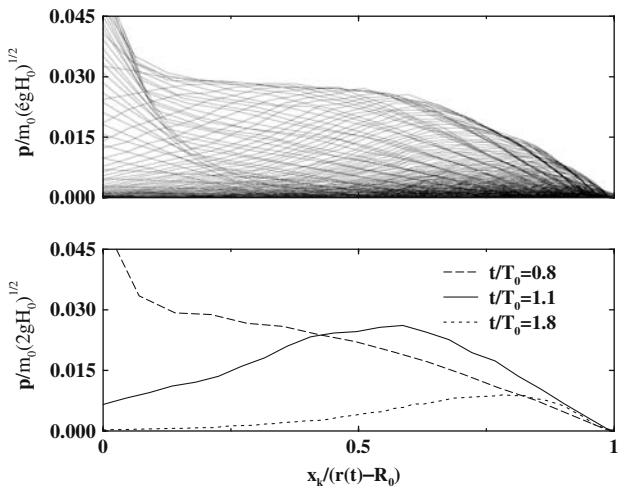

Fig. 13 Successive profiles of the momentum in the course of the spreading plotted every 0.0125s (*top*) and at three different moments of the spreading (*bottom*) as a function of the normalised position in the flow for $a = 11.7$ and $\mu = 0.01$

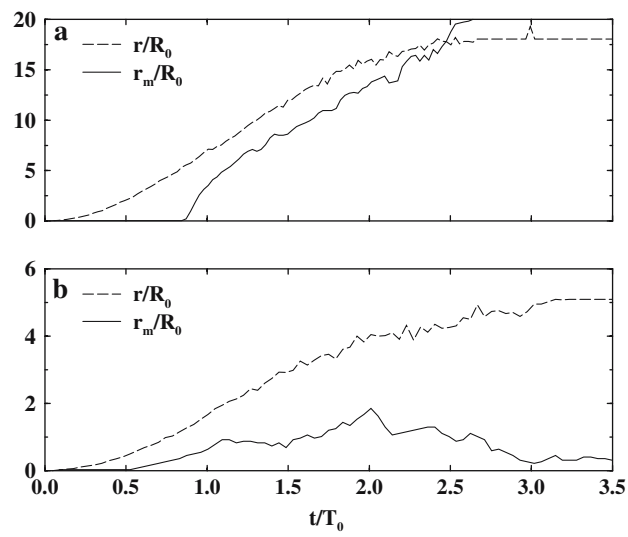

Fig. 14 Normalised position $(r - R_0)/R_0$ of the front of the flow (*dashed line*) and normalised position $(r_m - R_0)/R_0$ of the momentum wave in the course of the normalised time t/T_0, for an aspect ratio $a = 11.7$ (*top graph*) and $a = 2.2$ (*bottom graph*)

of the flow front $(r - R_0)/R_0$ in the course of time for two values of the aspect ratio $a = 11.7$ and $a = 0.73$. In the case $a = 11.7$, the momentum wave leaves the base of the column once the vertical collapse is over and rapidly propagates towards the front of the flow. On the contrary, for the small aspect ratios $a = 0.73$, the maximum of momentum remains located in the vicinity of the base of the column.

5.3 The effective friction: large aspect ratios

The mass distribution during the spreading necessarily plays a role in the dissipation process. As a result, considering the runout distance R_∞ or the position of the center of mass of the flow R_G to estimate the work of the friction forces is not equivalent for large aspect ratios. Evidence of this is given when plotting the normalised

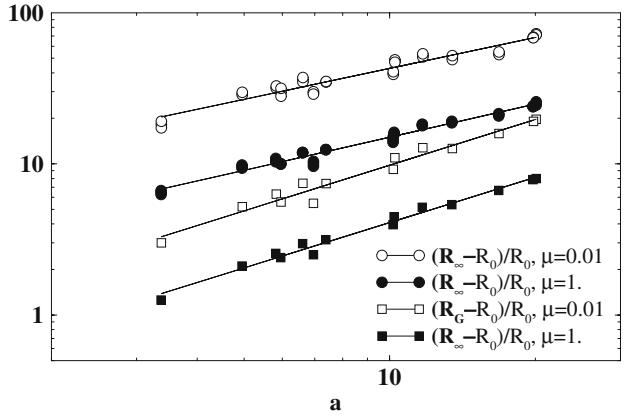

Fig. 15 Final normalised position of the center of mass $(R_G - R_0)/R_0$ (*square symbols*) and normalised runout distance $(R_\infty - R_0)/R_0$ (*circle symbols*) for inter-grain friction $\mu = 0.01$ and $\mu = 1$, and for aspect ratios such that $a > 2.5$

distance $(R_G - R_0)/R_0$ run by the center of mass during the spreading as a function of the aspect ratio a (Fig. 15): we no longer observe the power-law dependence given in (1), but we observe linear scalings showing:

$$(R_G - R_0)/R_0 \simeq \begin{cases} 0.62a^{1.0} & \mu = 0.01 \\ 0.24a^{1.0}, & \mu = 1. \end{cases} \tag{8}$$

The proportionality $(R_G - R_0) = \lambda H_0$ given by the scaling (8) allows us to define an effective coefficient of friction μ_e as done previously for small aspect ratios (Sect. 4.3). We suppose that the initial potential energy $\delta E = \frac{1}{2} m_0 g H_0$ is completely dissipated. The work of the friction force is given by $W_\mu = \mu_e m_0 g (R_G - R_0)$. Equating δE and W_μ leads to $\mu_e = (2\lambda)^{-1}$, where λ is the prefactor in the scaling (8).

This prediction gives $\mu_e = 0.8$ for $\mu = 0.01$ and $\mu_e = 2.08$ for $\mu = 1$, namely much higher values than those found in the case of collapses with small aspect ratios (Sect. 4.3). The reason is that supposing the initial potential energy to be entirely injected in the spreading dynamics is wrong; indeed, the multiple collisions occurring at the base of the column for large aspect ratios efficiently dissipate a great part of the energy, so that only a fraction is available for the sideways flow. In other words, we should write $\delta E = \frac{k}{2} m_0 g H_0$, with $k < 1$. If we assume that the effective friction properties of the sideways flow are the same for small and large aspect ratios, namely $\mu_e(0.01) = 0.14$ and $\mu_e(1) = 0.42$ following Sect. 4.3, we find that $k = 0.20$ and $k = 0.17$ respectively. Both values are close to what was obtained for similar numerical experiments [21]. Interestingly, the value of k seems to be only slightly dependent on the value of the inter-grain friction. At this point, the value of the restitution e is probably the relevant parameter.

6 Details of the velocity field

The value of the inter-grain friction μ is expected to affect the internal structure of the flow. To compare the two cases $\mu = 0.01$ and $\mu = 1$, we consider a vertical section of width $dx = 10D$ situated at a distance $(R_\infty - R_0)/3$ from the base of the column, and in which the velocity profile is measured. We have checked that this arbitrary choice for the location of the section did not qualitatively changed the results, beside the fact that measurements become less accurate when considering sections closer to the front due to the increasing shallowness of the flow and its shorter duration.

Figure 16a shows an example of the time evolution of the velocity profile for a column of aspect ratio $a = 11.7$. In the case $\mu = 1$, the profile can first be approximated by a plug flow, then turns to a linear profile with a zero velocity at the bottom, and eventually remains linear while a static deposit of increasing height h_d forms. The time evolution of the height of the deposit

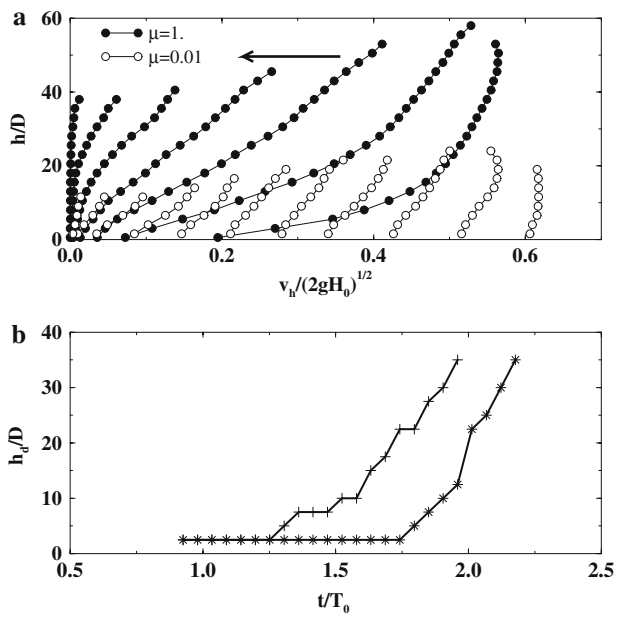

Fig. 16 **a** Normalised velocity profile of the flow $v_h/(2gH_0)^{1/2}$ as a function of the normalised depth h/D for time intervals of $\frac{1}{16}$ s., for $\mu = 1$ (*full circle*) and $\mu = 0.01$ (*empty circle*). The section where the profile is measured is situated at $r = r_\infty/3$, and the column is such as $a = 11.7$. The arrow shows the direction of increasing time. **b** Normalised thickness h_d/D of the static layer forming at the bottom of the flow displayed in (**a**) with $\mu = 1$ in the course of the normalised time. The two symbols corresponds to two different velocity criteria for tracking h_d (see text for details)

h_d is plotted in Fig. 16b. The two different symbols stand for two different criteria for tracking h_d: indeed, grains at the top of the static layer are not strictly static in the sense that they have a mean agitation, and their identification will depend on the velocity criteria adopted. The symbols + correspond to a velocity threshold of $(gD)^{1/2}$, while $*$ symbols correspond to a velocity threshold $(gD)^{1/2}/10$. In both cases, we observe the gradual growth of the static layer until the whole section comes to a rest, as already observed by [11]. These general features of the velocity profile are apparent in Fig. 17 where the deformation of an initial vertical section of grains is shown in the course of the spreading for $\mu = 1$.

In the case $\mu = 0.01$, the profile is mainly linear with a decreasing but non-zero velocity at the bottom. By contrast with the case $\mu = 1$, we are not able to track the growth of a static deposit due to the very short time during which it forms. Relative to the duration of the flow, the formation of the static deposit and the freezing of the flow are quasi-instantaneous.

The influence of μ is also visible in the evolution of the shear rate $\gamma = \Delta v/\Delta h$, where Δv is the variation of velocity in the section of the flow over the flowing depth $\Delta h = h - h_d$. For both values of the inter-grain friction μ, γ varies in the course of time, and no clear stationary regime is achieved.

In the case $\mu = 1$, we compute γ only from the time t_i on at which velocity profiles tend to be linear (we can show that $t_i \propto T_0$). The evolution of the normalised shear rate $\gamma(D/g)^{1/2}$ is plotted as a function of the normalised time $(t - t_i)/T_0$ in Fig. 18 for different values of the aspect ratio a. All the plots show a slow decrease and roughly collapse following a main tendency which is well approximated by:

$$\gamma(D/g)^{1/2} \simeq -0.14(t - t_i)/T_0 \quad (+0.13). \tag{9}$$

The important dispersion occurring for increasing time reflects the large uncertainties in the evaluation of Δh, due to the evaluation of the height h_d of the static layer building up while the flow is slowing down.

For $\mu = 0.01$ (Fig. 19), $\gamma(D/g)^{1/2}$ in no longer monotonic. It first increases, and then decreases up to the time t_f for which the layer becomes static. When plotting the evolution of $\gamma(D/g)^{1/2}$ as a function of the normalised time $(t - t_f)/T_0$, the decreasing part of the plots roughly

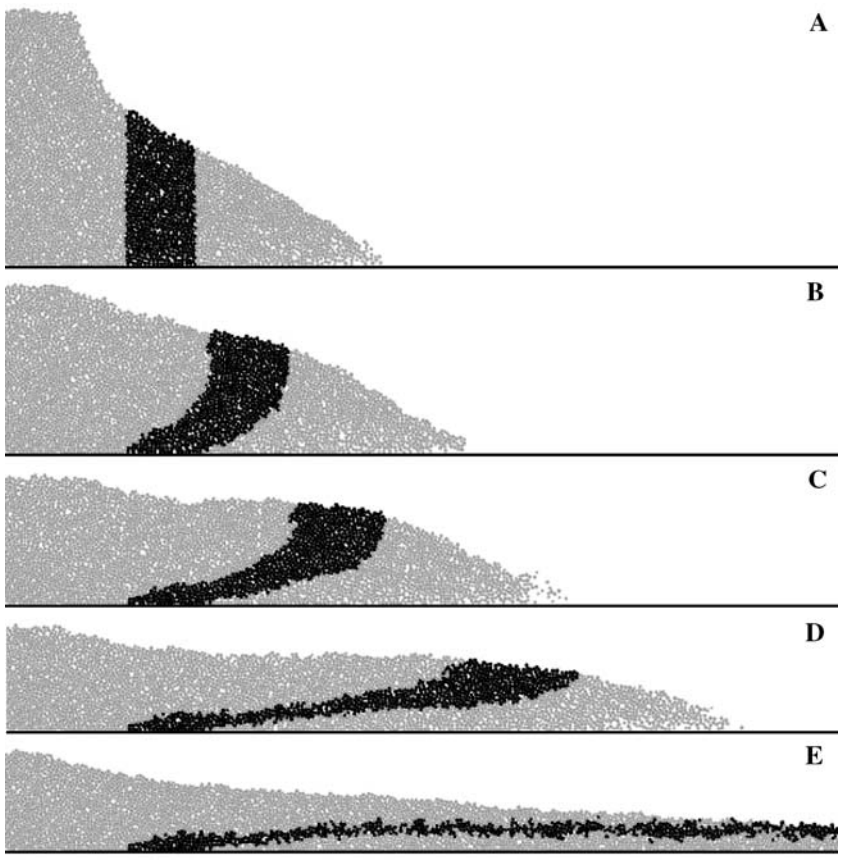

Fig. 17 Deformation of a vertical section of grains in the course of the spreading reflecting the velocity profile, for $\mu = 1$ and $a = 11.7$. In particular one can recognize the formation of a static layer in the stretching of the section. Snapshots are taken at the following successive times $t/T_\infty = 0.30$, 0.4, 0.55, 0.65 and 1

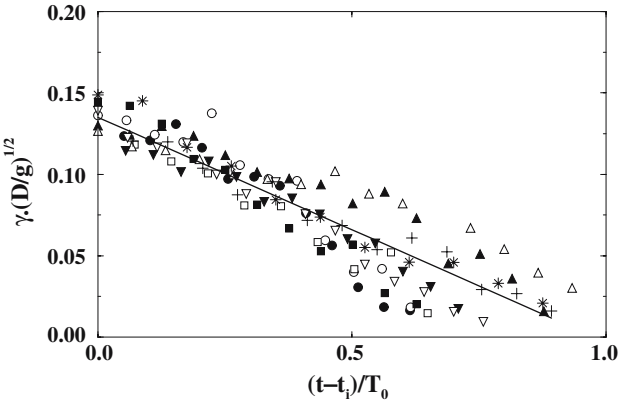

Fig. 18 Normalised shear rate $\gamma(D/g)^{1/2}$ as a function of the normalised time $(t - t_i)/T_0$, for $\mu = 1$ and $a = 20$, 16.8, 13.4, 11.7, 10.2, 10.1, 7.4, 6.6, 5.8 and 4.9 corresponding to 3 different values of the initial radius R_0

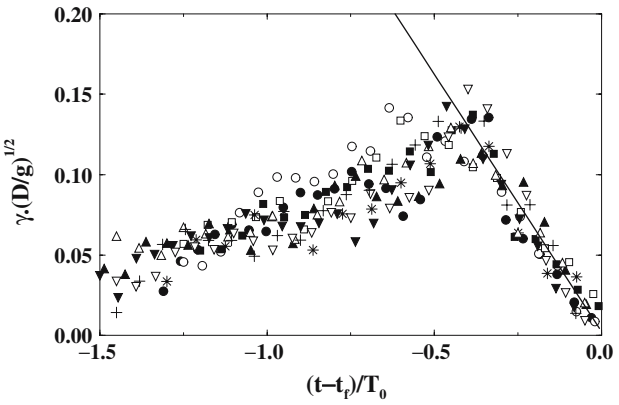

Fig. 19 Normalised shear rate $\gamma(D/g)^{1/2}$ as a function of the normalised time $(t - t_f)/T_0$, for $\mu = 0.01$ and $a = 20$, 16.8, 13.4, 11.7, 10.2, 10.1, 7.4, 6.6, 5.8 and 4.9 corresponding to 3 different values of the initial radius R_0

collapse following the tendency:

$$\gamma(D/g)^{1/2} = -0.32(t - t_f)/T_0. \tag{10}$$

These tendencies of the shear rate suggests that the evolution of the velocity profile is related to the initial condition through the emergence of the characteristic shear rate $(g/H_0)^{1/2}$ in the dependence given by (9) and by (10). These observations are in agreement with experimental observations by [15], but contrast with observations of [11] who worked with smaller aspect ratios for which the vertical dynamics is less determining.

However, the flow being non-stationary, relating its characteristics to the initial state is difficult and uncertain. As a consequence, assessing which of the initial condition or of the properties of the grains is actually determining the internal structure of the flow is not straightforward. In any case, the inter-grain friction μ has a paramount influence and induces significant differences. It is interesting that these differences do not affect the general behaviour of the runout in the sense that the dependence of the aspect ratio given by the scaling (1) is the same irrespective of the value of μ.

7 Summary and discussion

In this paper we have presented 2D numerical simulations of the collapse and the spreading of a granular mass in which both the effects of the initial condition and the effects of the details of the interactions between the grains were investigated. The experiment was similar to previous setup used in [21,22,11,14] and consists of suddenly releasing column of grains onto an horizontal plane and letting it spread freely until it comes to rest as a deposit of various shape and runout.

We first observed that the coefficient of restitution e was dramatically changing the behaviour of the systems for $e \to 1$; in particular, this dramatic change is expected to become more important for increasing values of a. On the contrary, for $e \leq 0.8$, the influence of the coefficient of restitution becomes negligible. Considering these results, we focused our analysis on the influence of the inter-grain friction μ only, in a wide range of values, namely from $\mu = 0.01$ to $\mu = 2$. The scaling for the runout distance showed both a linear and a power-law dependence on the aspect ratio of the initial column, in agreement with previous findings [21,22,11,14], and independently of the value of μ. Analyzing the early stage of the collapse, we show that free-fall dynamics is driving the spreading process providing the aspect ratio is large enough, and is only slightly sensitive to the value of μ. Its occurrence coincides with the transition from linear to power-law dependence of the runout. For small aspect ratio, the spreading results from a Coulomb-like failure of the edges and imply no free fall of the column. In this case, the effective friction properties of the flow can be simply predicted from the shape of the final deposit. The effective coefficient of friction μ_e was computed and plotted as a function of the inter-grain friction μ. For large values of μ, the effective properties saturates and μ_e no longer varies with μ. On the contrary, small values of μ induce an important lubrication of the flow and the rapid drop of the effective friction.

For large aspect ratios, in which we were mainly interested, the dissipation process is more complex due to the free-fall dynamics. Indeed the vertical acceleration of the grains induces a non-trivial mass distribution in the flow while propagating. This mass distribution plays a dominant role in the power-law scaling law obeyed by

the runout. Indeed, when considering the final position of the center of mass of the deposit instead of the runout distance, namely when accounting for the mass distribution, one obtain a linear scaling with a and no longer a power-law.

Finally, we have shown that the value of the intergrain friction μ was deeply affecting the internal structure of the flow. In particular, large inter-grain friction leads to the gradual growth of a static layer at the base of the flow, while small inter-grain friction does not allow this static layer to build up, and the flow freezes in a very short time.

It should be noted that the collapse experiment is highly transient and no clear stationary regime was observed. On the contrary, the acceleration and the deceleration phases cover nearly the whole duration of the spreading. This makes the analysis of the structure of the flow and its relation with other characteristic of the system uneasy.

Considering this, we were able to show nevertheless how the initial condition was dominating the behaviour of the spreading through the mass distribution induced in the flow. This means that the knowledge of the final runout is not a sufficient characterization of the deposit: one also needs to know how mass is distributed to understand the dynamics and the dissipation process. This is expected to be true in natural contexts as well as in experiments.

While the inter-grain friction μ does not affect the early vertical dynamics, nor the power-law dependence, it controls the effective frictional properties of the flow, and its internal structure. It is interesting to note that the details of the structure of the flow do not influence the final runout dependence, and thus seem to play a marginal role in the overall behaviour of the spreading. This could explain why simple shallow-water model with basic rheology but where the free-fall dynamics was accounted for could reproduce the runout scalings [12]. At this stage, it appears that the collapse experiment for large aspect ratios mixes two very different dynamics: while the second stage consists of a "conventional" horizontal granular flows, the first stage implies a large vertical acceleration. It shows how the initial condition can be repercuted in the overall behaviour of a granular system, and suggests that triggering mechanisms play a crucial role in the case of natural flows. This stresses the necessity of accounting for vertical acceleration in continuum models in the perspective of producing realistic prediction of the behaviour of granular flows.

References

1. Aranson, I.S., Tsimring, L.S.: Continuum descrition of avalanches in granular media. Phys. Rev. E **64**, R020301 (2001)
2. Balmforth, N.J., Kerswell, R.R.: Granular collapse in two dimensions. J. Fluid Mech. **538**, 399–428 (2004)
3. Cleary, P.W., Campbell, C.S.: Self-lubrication for long run-out landslides: examination by computer simulation. J. Geophys. Res. **98**(21), 911–924 (1993)
4. Cundall, P., Stack, O.: Geotechnique **29**(1), 47 (1979)
5. Dade, W.B., Huppert, H.E.: Long-runout rockfalls. Geology **26**, 803–806 (1998)
6. Douady, S., Andreotti, B., Daerr, A.: On granular surface flow equations. Eur. Phys. J. B **11**, 131 (1999)
7. Gray, J.M.N.T., Wieland, M., Hutter, K.: Gravity-driven free surface flow of granular avalanches over complex basal topography. Proc. R. Soc. Lond. **445**, 1841–1874 (1999)
8. Iverson, R.M.: The physics of debris flows. Rev. Geophys. **35**, 245–296 (1997)
9. Jean, M.: Frictional Contact in Rigid or Deformable Bodies: Numerical Simulation of geomaterials. pp. 463–486. In: Salvadurai, A.P.S., Boulon, J.M. (eds.) Elsevier, Amsterdam (1995)
10. Lajeunesse, E., Mangeney-Castelneau, A., Vilotte, J.-P.: Spreading of a granular mass on an horizontal plane. Phys. Fluids **16**, 2731–2381 (2004)
11. Lajeunesse, E., Monnier, J.B., Homsy, G.M.: Granular slumping on a horizontal surface. Phys. Fluids **17**, 103302 (2005)
12. Larrieu, E., Staron, L., Hinch, E.J.: Raining into shallow water as a description of the collapse of a column of grains. J. Fluid Mech. (in press) (2005)
13. Lube, G., Huppert, H.E., Sparks, R.S.J., Hallworth, M.A.: Axisymmetric collapses of granular columns. J. Fluid Mech. **508**, 175–199 (2004)
14. Lube, G., Huppert, H.E., Sparks, R.S.J., Freundt, A.: Collapse of granular columns. Phys. Rev. E **72**, 041301 (2005)
15. Lube, G., The flow and depositional mechanisms of granular matter, PhD Thesis, University of Kiel, Germany (2006)
16. Midi, G.D.R.: On dense granular flows. Eur. Phys. J. E **14**, 341–365 (2004)
17. Moreau, J.-J.: Some numerical methods in multibody dynamics: application to granular materials. Eur. J. Mech. A/Solids **4**, 93–114 (1994)
18. Pouliquen, O., Forterre, Y.: Friction law for dense granular flows: application to the motion of a mass down a rough inclined plane. J. Fluid Mech. **453**, 133–151 (2002)
19. Rajchenbach, J.: Granular flows. Adv. Phys. **49**(2), 229–256 (2000)
20. Savage, S., Hutter, K.: The motion of a finite mass of granular material down a rough incline. J. Fluid Mech. **199**, 177–215 (1989)
21. Staron, L., Hinch, E.J.: Study of the collapse of granular columns using two-dimensional discrete-grains simulation. J. Fluid Mech. **545**, 1–27 (2005)
22. Zenit, R.: Computer simulations of the collapse of a granular column. Phys. Fluid **17**, 031703 (2005)